Applied Catalysis B: Environmental 142–143 (2013) 396–405

Contents lists available at SciVerse ScienceDirect

Applied Catalysis B: Environmental

journal homepage: www.elsevier.com/locate/apcatb

Degradation of chlorophenols using a novel Fe^0/CeO_2 composite

L.J. Xu [a], J.L. Wang [a,b,*]

[a] Laboratory of Environmental Technology, INET, Tsinghua University, Beijing 100084, PR China
[b] Beijing Key Laboratory of Fine Ceramics, Tsinghua University, Beijing 100084, PR China

ARTICLE INFO

Article history:
Received 18 January 2013
Received in revised form 24 May 2013
Accepted 26 May 2013
Available online 1 June 2013

Keywords:
Fe^0/CeO_2 composite
Degradation
Removal
Reaction mechanism
Chlorophenols

ABSTRACT

A novel Fe^0/CeO_2 composite was synthesized, characterized and applied for removal of different kinds of chlorophenols, including 4-chlorophenol (4-CP), 2,4-dichlorophenol (2,4-DCP), 2,4,6-trichlorophenol (2,4,6-TCP) and pentachlorophenol (PCP). Fe^0/CeO_2 composite was prepared by the impregnation method, their physicochemical properties were characterized before and after reaction by X-ray diffraction (XRD), scanning electron microscopy (SEM) with energy-dispersive X-ray spectrometer (EDX), high-resolution transmission electron microscopy (HRTEM), the Brunauer–Emmett–Teller (BET) method, X-ray photoelectron spectroscopy (XPS), and Raman spectroscopy. The results showed that spherical zero-valent iron particles ranged in 200–400 nm were dispersed on ceria matrix. The BET surface area and pore volume of synthesized Fe^0/CeO_2 composite were 16.76 m^2/g and 0.056 cm^3/g, respectively. The introduction of CeO_2 facilitated the generation of chemisorbed oxygen on the surface and the dissolution of Fe^0. 2,4-DCP was adsorbed on the Fe^0/CeO_2 surface, reductive dechlorinated by Fe^0 and Fe^{2+}, and/or oxidative degraded by hydroxyl radicals (•OH), superoxide radicals ($O_2^{\bullet-}$), and H_2O_2 species. Additionally, the extent of chlorophenols removal, TOC removal and dechlorination followed the order of PCP > 2,4-DCP > 2,4,6-TCP > 4-CP.

© 2013 Elsevier B.V. All rights reserved.

1. Introduction

Chlorophenols, including 4-chlorophenol (4-CP), 2,4-dichlorophenol (2,4-DCP), 2,4,6-trichlorophenol (2,4,6-TCP) and pentachlorophenol (PCP), are widely employed in many industrial processes and used as fungicides, herbicides, defoliants, disinfectants and preservative agents [1,2]. Because of their toxicity, carcinogenicity and bioaccumulation, their disposal is currently one of the most serious environmental problems [3,4].

Different alternative methods have been developed for the destruction of organic pollutants in water, and the available methods mainly use various catalysts, such as Ti–Al-containing mesoporous silicas [4], Fe_3O_4 magnetic nanoparticles [5], zero valent zinc [6], Pd/C [7], Mg/Pd [8] and Ni/Fe [9] bimetallic particles. Among these catalysts, zero-valent iron (Fe^0), capable of inducing reductive transformation of organic compounds or driving oxidative degradation by activating oxygen (O_2) to generate strong oxidants, provides a new approach for the treatment of aquatic contaminants. Over the past decade, Fe^0 has been used to dehalogenation of halogenated compounds [10–12], denitrification of nitroaromatic compounds [13], reduction of pesticides [14], and oxidative degradation of organics [15–17]. However, in the absence of additives or catalysts, the efficiency of the Fe^0–O_2 system is relatively low, limiting the applicability of this approach to contaminants treatment. Recently, ceria (CeO_2) has been suited to and widely used as catalyst support or active species due to its elevated oxygen storage capacity and redox and catalytic properties [18–20]. These unique properties can be augmented by the addition of transition metals, and the performance of ceria-supported metal/metal oxide catalysts is enhanced not only by creating more vacancies but also by inducing more redox couples in the transition metals as well as in the ceria [18,20–22]. Our previous study showed that the catalytic activity of nanoscaled Fe_3O_4/CeO_2 composite was much higher than that of either nanoscaled Fe_3O_4 or CeO_2 individually [22]. Although some different kinds of iron–cerium oxide composites have been synthesized and reported [18,23,24], few studies have explored the preparation of Fe^0/CeO_2 composite and its improved catalytic activity for removal of chlorophenols.

Contaminant removal in Fe^0–H_2O systems is the result of a complex interplay of physical adsorption and co-precipitation processes, electrochemical reduction and chemical oxidation [17,25–28]. The mechanism of reductive transformation has been well-established, and the produced reductive species involve Fe^0, Fe^{2+}, H/H_2, iron hydroxides and oxides [25,26]. The oxidative mechanism has been proposed by Sedlak's group [27–29], and the important oxidants formed in the Fe^0–O_2 system are superoxide radicals ($O_2^{\bullet-}$), hydroxyl radicals (•OH) and ferryl ions. The discussion over the relative importance of adsorption, reduction and oxidation on the process of contaminant removal is still

* Corresponding author at: Neng Ke Lou, Tsinghua University, Beijing 100084, PR China. Tel.: +86 10 62784843; fax: +86 10 62771150.
E-mail address: wangjl@tsinghua.edu.cn (J.L. Wang).

0926-3373/$ – see front matter © 2013 Elsevier B.V. All rights reserved.
http://dx.doi.org/10.1016/j.apcatb.2013.05.065

ongoing, and the contribution of these generated reactants needs to be determined. Noubactep [26] demonstrated that contaminant removal in Fe^0–H_2O systems was a synergistic effect of adsorption, co-precipitation and reduction. Stieber et al. [17] suggested that reductive and oxidative processes were responsible for the treatment of pharmaceuticals and diagnostic agents with zero-valent iron in the presence of oxygen. Furthermore, the behavior of CeO_2 in the application of Fe^0/CeO_2 composite for chlorophenols removal requires detailed investigation. Due to the different reaction mechanisms during various treatment processes, the relationship between the structures of chlorophenols and the removal rates remains controversial, and this also needs to be further studied.

In this study, Fe^0/CeO_2 composite was synthesized and characterized using a number of techniques to investigate changes of the catalyst before and after reaction and to further understand the structure–activity relationship. The catalytic activity test reaction of Fe^0/CeO_2 composite was investigated by the removal of 2,4-DCP under various reaction conditions, and the interpretation for the observations was proposed. Moreover, whether various chlorophenols were transformed and removed by Fe^0/CeO_2 composite in oxic solutions was also examined.

2. Materials and methods

2.1. Chemicals

Cerium (III) nitrate hexahydrate ($Ce(NO_3)_3{\cdot}6H_2O$), polyethylene glycol (PEG) 4000 (Sinopharm Chemical Reagent Co., Ltd.), and ammonium carbonate ($(NH_4)_2CO_3$, Beijing Yili Fine Chemical Factory) were used for the preparation of CeO_2. Ferrous sulfate ($FeSO_4{\cdot}7H_2O$) was purchased from Shenyang Reagent Factory, and kalium borohydride (KBH_4) was obtained from Nankai Fine Chemical factory. 4-CP, 2,4-DCP, 2,4,6-TCP and PCP were supplied by Tianjin Jinke Fine Chemical Industry Research Institute, Beijing Jinlong Chemical Reagent Co., Ltd., Alfa Aesar (USA), and Beijing Shiying Chemical Factory, respectively. Sulphuric acid (H_2SO_4) and *n*-butanol were obtained from Beijing Chemical Factory. Catalase and *p*-benzoquinone came from the Sigma-Aldrich Co. LLC. Argon (Ar) gas was supplied by Beijing Aolin Gas Company. All chemicals were of analytical grade, and double distilled water was employed throughout this study.

2.2. Preparation and characterization of Fe^0/CeO_2 composite

CeO_2 particles were precipitated from $Ce(NO_3)_3{\cdot}6H_2O$ solution with PEG 4000 using $(NH_4)_2CO_3$ aqueous solution, as described elsewhere [22]. Fe^0/CeO_2 composite was prepared by the impregnation method with a calculated amount of CeO_2 particles according to our previous work [22,30]. A 100 mL of 0.2 M KBH_4 aqueous solution was added dropwise to a four-necked flask containing 100 mL of 0.04 M $FeSO_4{\cdot}7H_2O$ and 0.22 g CeO_2 with violent stirring under Ar protecting at ambient temperature. After 1.5 h of reaction, the synthesized particles with the weight ratio of Fe^0 and CeO_2 1:1 were deposited and washed with deionized water for two times, and finally dried at room temperature under vacuum for instant usage.

X-ray diffraction (XRD) measurement was taken by an X-ray powder diffractometer (D8-Advance, Bruker, 40 kV and 40 mA, Cu Kα) at room temperature over a range of 15–90° at a scan speed of 8°/min. The morphology of samples was determined by a field emission scanning electron microscope (SEM, JSM-6301F, JEOL) with energy-dispersive X-ray (EDX) detector, and a high-resolution transmission electron microscopy (HRTEM, Tecnai G2 F20 S-Twin). The Brunauer–Emmett–Teller (BET) specific surface area and the Barret–Joyner–Halenda (BJH) pore size distribution of catalysts were measured by N_2 adsorption–desorption measurements at 77 K using a Micromeritics NOVA 3200e BET sorptometer after degassing the samples at 80 °C for 5 h. X-ray photoelectron spectroscopy (XPS) measurement was performed using a PHI-5300 system with an Al Kα radiation (1486.6 eV), and the software package XPSpeak 4.1 was used for data analysis. Raman spectra were recorded with a Perkin Elmer Spectrum GX spectrometer equipped with a 750 nm laser source.

2.3. Experimental procedure

The experiments were performed in conical flasks (25 mL) that were unsealed and saturated with air to maintain oxic conditions. For anoxic experiments, the conical flasks were capped and sealed with parafilm before reaction. These conical flasks were placed on a rotary shaker (TZ-2EH, Beijing Wode Company) with an agitation of 150 rpm at 30 °C in the dark. The reaction suspension containing 1.0 g/L Fe^0/CeO_2 composite and 10 mL of 50 mg/L chlorophenol solution was prepared, and its initial pH was adjusted by H_2SO_4. At each specific sampling time, aqueous sample was withdrawn by a 5 mL syringe, and filtered immediately by a 0.22 μm filter film to remove the catalyst particles before analysis. All experiments were repeated at least two times, and averages are reported.

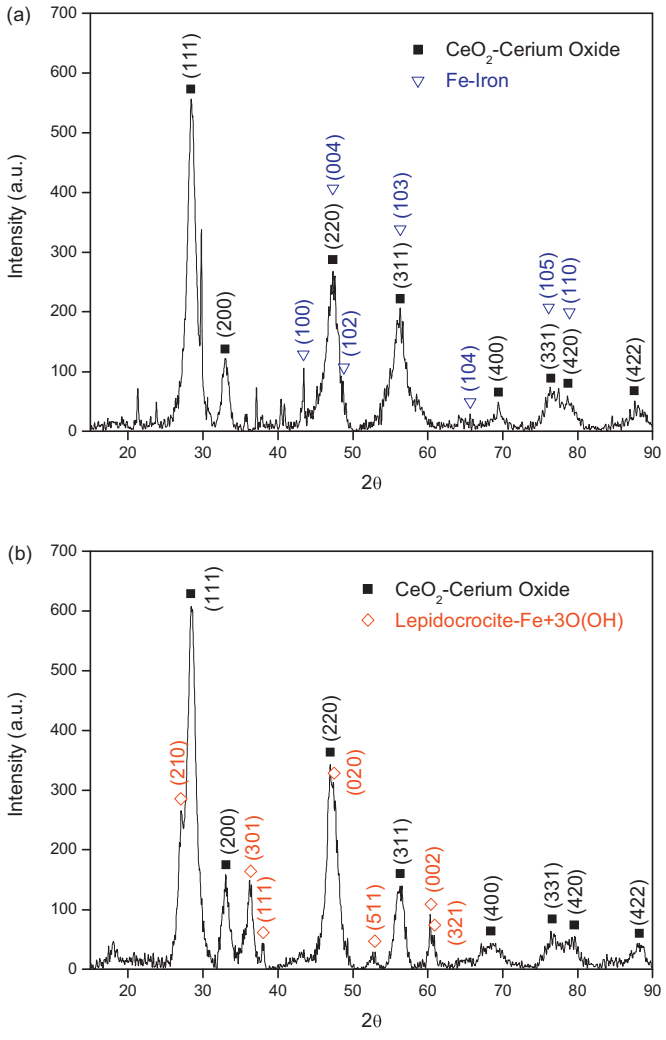

Fig. 1. XRD patterns of Fe^0/CeO_2 composite before (a) and after reaction (b).

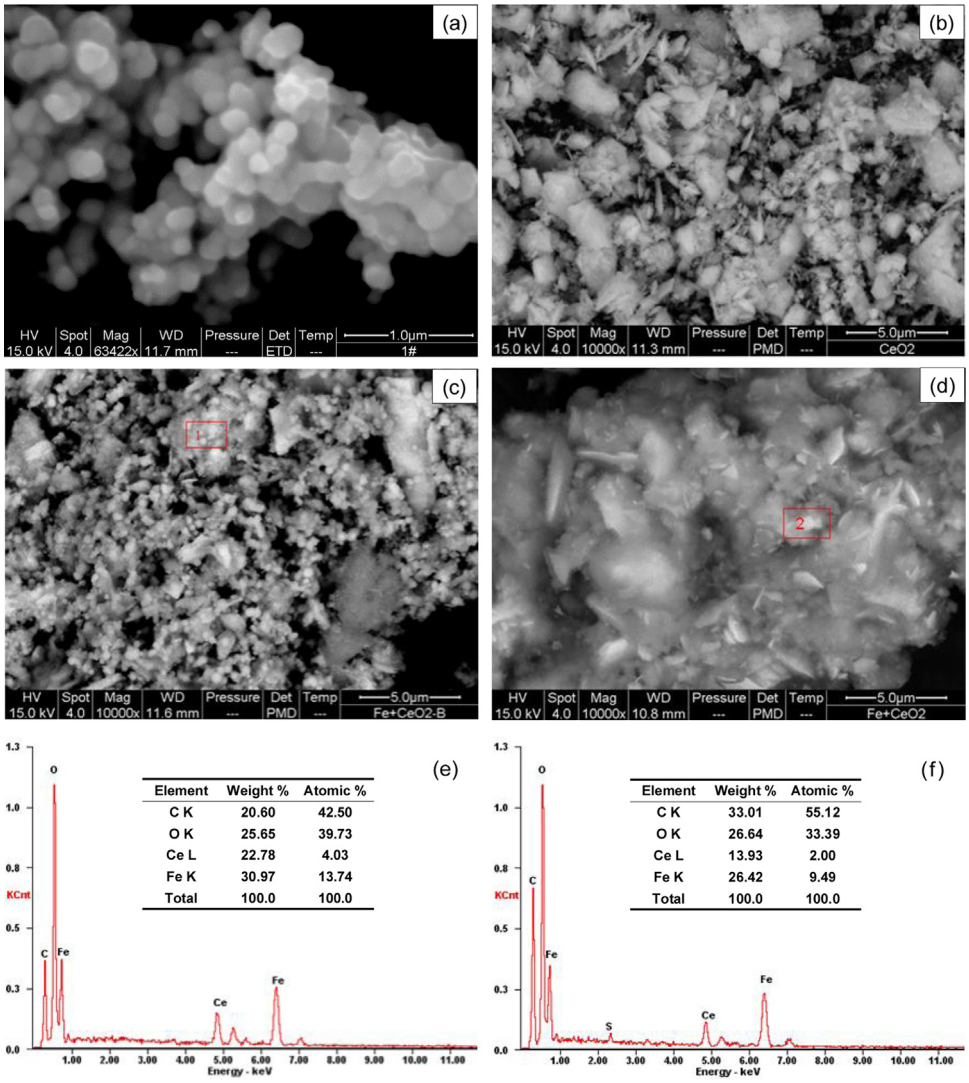

Fig. 2. SEM micrographs of (a) synthesized nanoscaled Fe^0, (b) synthesized CeO_2 powders, (c) Fe^0/CeO_2 composite before reaction, (d) Fe^0/CeO_2 after reaction, and EDX data with component ratios (inset) of Fe^0/CeO_2 composite before (e) and after reaction (f).

2.4. Sample analysis

Quantitative analysis of chlorophenols was done using a high performance liquid chromatograph (HPLC Agilent 1200) equipped with a diode array detector (DAD) and a C18 reversed-phase column (5 μm, 4.6 mm × 150 mm). The testing conditions were (a) water and methanol (40:60, v/v) as the mobile phase with a flow rate of 1.0 mL/min at the analytical wavelength of 280 nm for 4-CP, and 254 nm for phenol and 2-chlorohydroquinone, (b) water and methanol (30:70, v/v) with 1.0 mL/min at 284 nm for 2,4-DCP and 2,4,6-TCP, and (c) water and methanol (25:75, v/v) with 0.8 mL/min at 320 nm for PCP. The extent of mineralization was determined by a Multi 2100 TOC/TN analyzer (Analytik Jena AG Corporation). The pH was measured with a Thermo Orion model 8103BN pH-meter. Chloride ions (Cl^-) and carboxylic acids were analyzed using a Dionex DX-100 ion chromatography coupled with a Dionex RFIC™ IonPac® AS 14 analytical column (4 mm × 250 mm) and a Dionex RFIC™ IonPac® AG 14 guard column (4 mm × 50 mm). An eluent solution, containing 3.5 mM Na_2CO_3 and 1.0 mM $NaHCO_3$, was pumped at a flow rate of 1.0 mL/min. The dissolved iron and cerium concentrations were detected by atomic absorption spectrometry (TAS990).

Table 1
Structural parameters of Fe^0, CeO_2 and Fe^0/CeO_2 samples.

Sample	S_{BET} (m^2/g)	V_P (cm^3/g)	D_P (nm)
Fe^0	3.89	0.01	3.72
CeO_2	108.03	0.096	3.82, 19.72
Fe^0/CeO_2	16.76	0.056	3.83, 19.19

3. Results and discussion

3.1. Crystal structure

XRD patterns of pure CeO_2 particles and nanoscaled Fe^0 are described in detail elsewhere [22,30]. Fig. 1a shows the crystal structure of Fe^0/CeO_2 composite. The XRD patterns of CeO_2 crystallized in a cubic fluorite structure (JCPDS 65-5923) with space group *Fm*3*m* (225) were dominant, which showed peaks at 2θ values of 28.6°, 33.1°, 47.6°, 56.4°, 69.5°, 76.8°, 79.2° and 88.6° corresponding to (111), (200), (220), (311), (400), (331), (420) and (422) crystal planes, respectively. Iron also appeared with a hexagonal structure (JCPDS 50-1275) with space group *P*, as evidenced by the weak diffraction peaks from the (100), (004), (102), (103), (104), (105) and (110) planes at 43.0°, 47.4°, 49.4°, 56.7°, 65.9°, 76.9° and 78.8°, respectively [31], most of which coincided with the

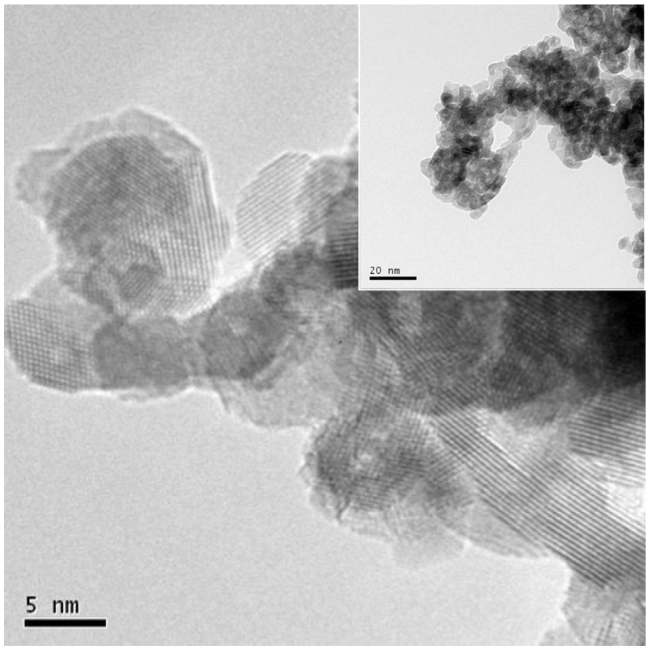

Fig. 3. HRTEM images of CeO_2 particles.

patterns of CeO_2. Thus, the XRD spectroscopy analysis suggested that the Fe^0/CeO_2 composite was crystallized out with cubic fluorite structural form of CeO_2, which is similar with the results reported by other researchers [32,33].

As seen in the XRD patterns of Fe^0/CeO_2 composite after 24 h of reaction (Fig. 1b), the characteristic peaks of CeO_2 did not change obviously before and after reaction. The formation of iron oxides was observed after reaction, possibly associated with lepidocrocite (γ-FeOOH, JCPDS 44-1415). In the presence of oxygen as electron acceptor, iron (III) oxyhydroxides are formed as corrosion products of Fe^0, which may be lepidocrocite or some mixture of lepidocrocite and $Fe(OH)_3$ [30,34,35].

3.2. Morphology of samples

As shown in the typical SEM image of the synthesized Fe^0 (Fig. 2a), the iron particles were composed of spherical particles with size distribution within 100–200 nm. Fig. 2b indicates the presence of CeO_2 particles that does not display any definite surface morphology. Combined with HRTEM images (Fig. 3), the primary CeO_2 particles are nanoscaled and appear to be aggregated into larger plate-like particles. As the zero-valent iron and cerium oxide particles present in the mixed oxide had different shapes, the dispersion of Fe^0 particles on ceria matrix was suggested from Fig. 2c. Grain sizes of Fe^0 in the Fe^0/CeO_2 composite were larger than that of the pure Fe^0, which ranged in 200–400 nm. EDX analysis in a SEM was performed on the Fe^0/CeO_2 crystalline materials to evaluate their elemental contents. Fig. 2e shows the EDX data acquired from a region of Fe^0/CeO_2 composite before reaction (region 1 in Fig. 2c), which reveals that the concentrations of Ce and Fe on the Fe^0/CeO_2 surface were 22.78 wt.% and 30.97 wt.%.

After 24 h of reaction, the flake-like structural crystals appeared as seen in Fig. 2d, suggesting the formation of iron oxides and further coprecipitation resulting from iron corrosion in water. These corrosion products were likely composed of lepidocrocite (γ-FeOOH) [35,36], which corroborates the XRD results. According to EDX quantification (Fig. 2f), the weight percentages of Ce and Fe after reaction were 13.93% and 26.42%. Slight decrease was noticed between the samples before and after reaction, indicating that small amount of Ce and Fe was lost after reaction. The concentrations of dissolved Fe and Ce in the solution after 24 h of reaction were 9.85 and 0.21 mg/L, respectively.

3.3. BET surface area

The nitrogen adsorption/desorption measurements were also performed to investigate the specific surface areas and characteristics porosity of catalysts as summarized in Table 1. The BET isotherm of Fe^0/CeO_2 composite (Fig. 4a) exhibited type-IV isotherms with H3 type hysteresis loops according to the Brunauer–Deming–Deming–Teller (BDDT) classification, indicating the typical mesoporous structure of Fe^0/CeO_2 composite, and the existence of agglomerates of plate-like particles with slit shape pores in the sample [37,38]. Fig. 4b shows bimodal pore size distribution with the pore maxima centered at 3.83 and 19.19 nm, confirming that the Fe^0/CeO_2 composite is mainly mesoporous [39]. The peak at 3.83 nm is more intense, which might signify the higher adsorption in related region for Fe^0/CeO_2 composite [38]. The BET surface area (S_{BET}) of the composite was found to be 16.76 m^2/g, with corresponding pore volume (V_P) of 0.056 cm^3/g. Combined with the structural parameters of Fe^0 and CeO_2 particles (Table 1) as reported by our previous study [22], it was assumed that the contribution of introducing CeO_2 to pure Fe^0 particles brings about higher surface area and pore volume in the composite.

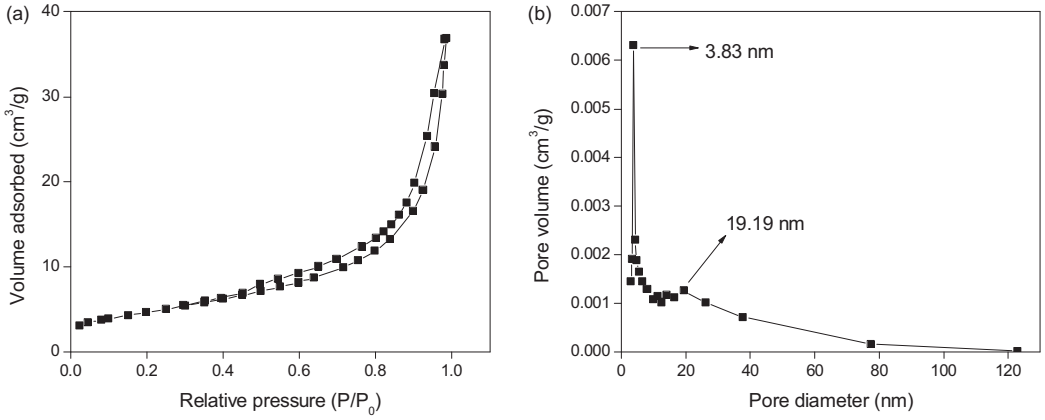

Fig. 4. Nitrogen adsorption/desorption isotherm (a) and BJH pore size distribution (b) of Fe^0/CeO_2 composite.

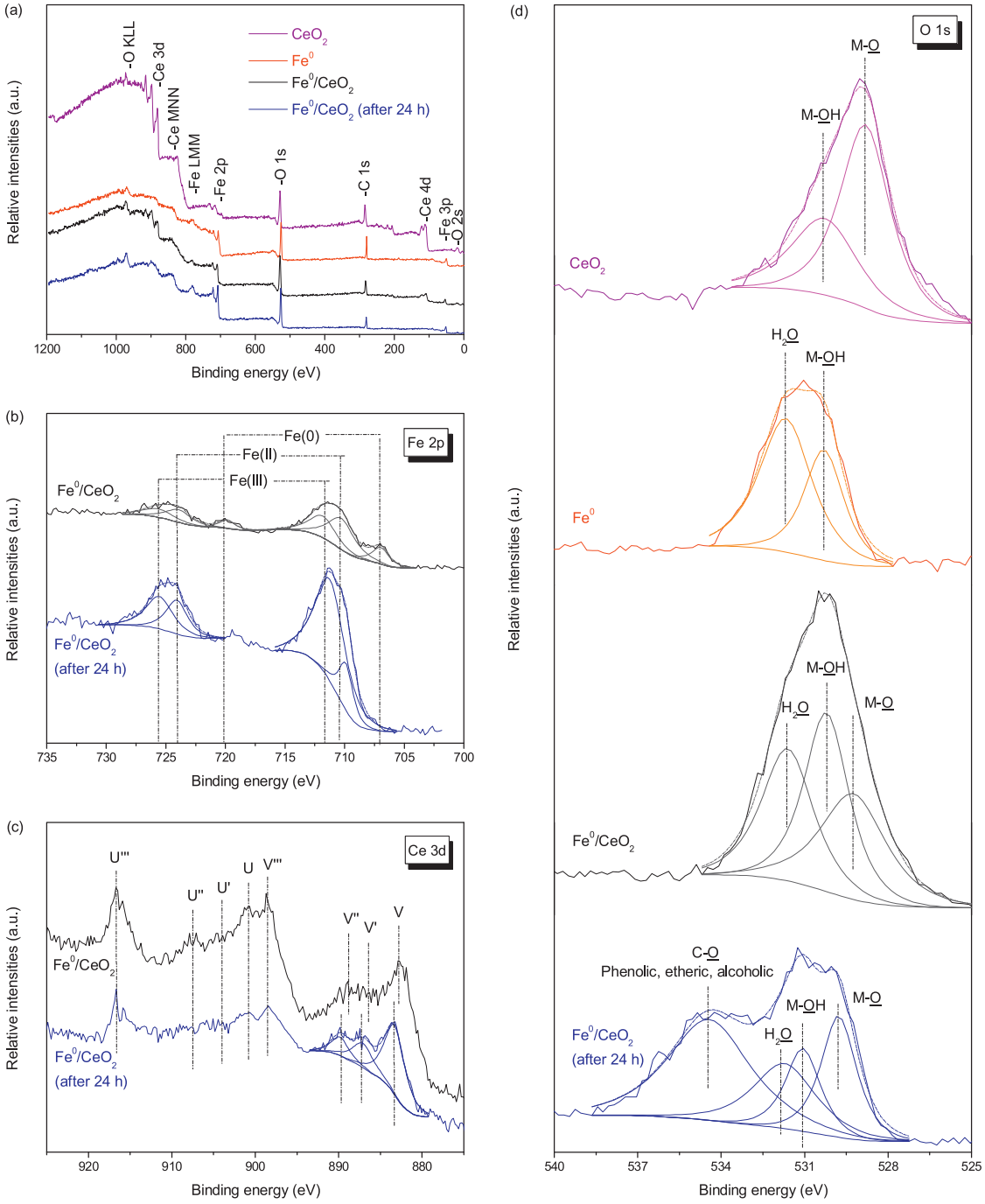

Fig. 5. XPS spectra of survey scan (a), and high-resolution scan of Fe 2p region (b), Ce 3d region (c) and O 1s region (d).

3.4. XPS analysis

Surface structure information of CeO_2, Fe^0, and Fe^0/CeO_2 composite before and after reaction was analyzed by XPS, and the spectra of both survey and high-resolution scans for the key elements of these samples are seen in Fig. 5. The peaks of binding energy (BE) for Fe 2p, Ce 3d, and O 1s were calibrated versus the carbon signal at 284.6 eV. From the survey spectra (Fig. 5a), the atomic ratios of C, O, Ce, and Fe on the surface of Fe^0/CeO_2 composite were 36.7%, 51.6%, 5.94%, and 5.76%, respectively, which differ from that measured by EDX elemental analysis (Fig. 2e), probably due to the fact that XPS probes the near surface region within about 5 nm compared to 1–2 μm for EDX [40].

Fig. 5b shows the high-resolution XPS spectra of Fe 2p region for Fe^0/CeO_2 composite before and after reaction. The photoelectron peaks of Fe $2p_{1/2}$ locate at 724.6 eV, and the Fe $2p_{3/2}$ peaks at around 712.0, 710.4 and 706.9 eV can be assigned to Fe(III), Fe(II) and Fe(0), respectively [22,41,42]. For Fe^0/CeO_2 composite, small Fe(0) peaks were present along with relatively strong peaks of oxidized iron, which suggested that the Fe^0 particles have a core–shell structure, consisting of a metallic iron (Fe^0) core surrounded by a thin layer of iron oxide/hydroxide [41,43]. As described in the literature [41,44], the overlayer is thought to form spontaneously during synthesis and handling of the composite in an aqueous solution. The Fe 2p photoelectron peak recorded from Fe^0/CeO_2 composite after 24 h of reaction shows that the Fe(0) peak disappeared, and the area of

Fe(II) decreased along with the increasing area of Fe(III), indicating the oxidation occurred on the composite surface.

High-resolution XPS spectra of Ce 3d region for Fe^0/CeO_2 composite before and after reaction are seen in Fig. 5c. Two pairs of spin-orbital doublets corresponding to the Ce $3d_{3/2}$ and Ce $3d_{5/2}$ states were labeled u and v, respectively [22,45]. The doublets labeled u/v, u″/v″, and u‴/v‴ represent the $3d^{10}4f^0$ initial electronic state of Ce^{4+}, while the u′/v′ doublet represents the $3d^{10}4f^1$ state corresponding to Ce^{3+} [46,47]. For Fe^0/CeO_2 composite, the peaks ascribed to Ce^{4+} were predominant. After 24 h of reaction, a small peak of v′ appeared, evidencing the presence of Ce^{3+}, which could create charge imbalance, the vacancies, and unsaturated chemical bonds on the catalyst surface, leading to the increase of chemisorbed oxygen on the surface [47,48].

From Fig. 5d, three peaks of the O 1s spectra positioned at around 529.2 eV, 530.3 eV, and 531.7 eV can be assigned to metal oxide or chemisorbed oxygen (M–O), hydroxyl bonded to metal (M–OH), and chemically or physically adsorbed H_2O (H_2O) on the catalyst surface, respectively [49–51]. For pure CeO_2, the BE peak of O 1s photoelectrons could be fitted into two peaks, one for M–O and another for M–OH. For Fe^0 particles, two peaks were contributed to M–OH and H_2O, and no peak for M–O was observed. Combined with the O 1s spectrum of Fe^0/CeO_2, the results suggest that the addition of CeO_2 in the Fe^0/CeO_2 composite should increase the area of M–O, resulting in the increase of chemisorbed oxygen on the surface that is the most active oxygen and plays an important role in oxidation reaction [47,48]. The existence of surface OH group observed on the Fe^0 and Fe^0/CeO_2 surface indicates the presence of FeOOH structure on both surfaces, which is in agreement with the result obtained from Fe 2p XPS spectra. Compared with the spectra of Fe^0/CeO_2 before and after reaction, it can be found that the area and height for the peak at 530.3 eV attributed to M–OH greatly decreased after reaction, suggesting that the M–OH groups on the catalyst surface participated in the removal of chlorophenols. Meanwhile, the area and height for the peak of chemisorbed oxygen on the surface increased after reaction, which might be due to the occurrence of Ce^{3+} according to the observation in the Ce 3d spectra. Thus, the Fe^0/CeO_2 composite might have a preferable activity for removal of organic compounds. It should be noted that a peak at a binding energy of 534.5 eV is attributed to carbonyl oxygen atoms in phenolic, etheric and alcoholic organics [52], further confirming that some organic pollutants were adsorbed or reacted on the catalyst surface.

3.5. Raman spectroscopy

Raman spectra of Fe^0/CeO_2 composite before and after reaction are reported in Fig. 6. It can be seen that Fe^0/CeO_2 composite shows a band centered at 453 cm^{-1} ascribed to the Raman active mode of CeO_2 [33,46]. After 24 h of reaction, there is a small shift of the band at 453 cm^{-1} to 456 cm^{-1}, and some extra peaks are observed at lower wavenumbers including 220, 285, 399, 603 and 1308 cm^{-1}. Based on the Raman signature, the bands at 220, 285 and 399 cm^{-1} may be attributed to goethite (α-FeOOH), and the band at 1308 cm^{-1} may be assigned to lepidocrocite (γ-FeOOH) [53,54]. The weak band at 603 cm^{-1} might be due to the C–Cl and C–O stretching and ring breathing [55], indicating the adsorption and co-precipitation of organic pollutants on the surface of the composite.

3.6. Removal of 2,4-dichlorophenol under various conditions

Control experiments were carried out to compare the removal of 2,4-DCP by CeO_2, Fe^0 and Fe^0/CeO_2 composite under anoxic and oxic conditions at initial pH 6.2 (solution original pH, not adjusted). As shown in Fig. 7, about 5% and 6% 2,4-DCP was diminished by

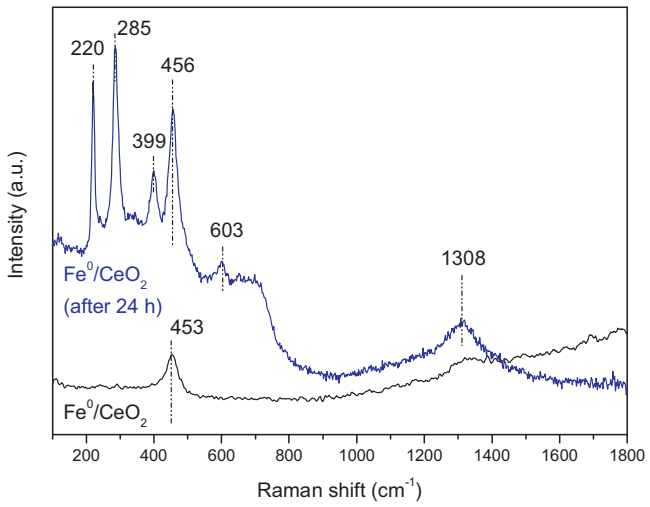

Fig. 6. Raman spectra of Fe^0/CeO_2 composite before and after reaction.

pure CeO_2 in the absence and presence of air, primarily ascribed to the surface adsorption of CeO_2. A slight removal of 2,4-DCP was observed by Fe^0 and Fe^0/CeO_2 composite in the early stage of the reaction, which was mainly attributed to surface adsorption. Higher adsorption of 2,4-DCP was achieved by Fe^0/CeO_2 than Fe^0, which could be resulted from the higher surface area and pore volume of Fe^0/CeO_2 composite as described in Section 3.3. After 24 h of reaction in anoxic solutions, 14% removal of 2,4-DCP was observed with 1.0 g/L Fe^0, and 18% removal of 2,4-DCP was obtained with 1.0 g/L Fe^0/CeO_2 composite. About 2.78 and 3.35 mg/L free chloride was detected in Fe^0 suspension and Fe^0/CeO_2 suspension, respectively, suggesting that the removal of 2,4-DCP under anoxic conditions was probably ascribed to both surface adsorption and reductive dechlorination [3,30].

In anoxic Fe^0–H_2O systems, three different pathways for reductive dechlorination are presented [17,25]. The first pathway involves the direct electron transfer from Fe^0 at the composite surface to the adsorbed chlorophenols (RCl) as seen in Eq. (1). The second pathway is the reduction by Fe^{2+} (Eq. (2)), which results from the corrosion of Fe^0 in aqueous systems. The third pathway for reductive dechlorination involves the catalytic hydrogenation by atomic hydrogen formed by iron corrosion with the reduction of H_2O via reaction (3). For Fe^0/CeO_2 composite, as shown in

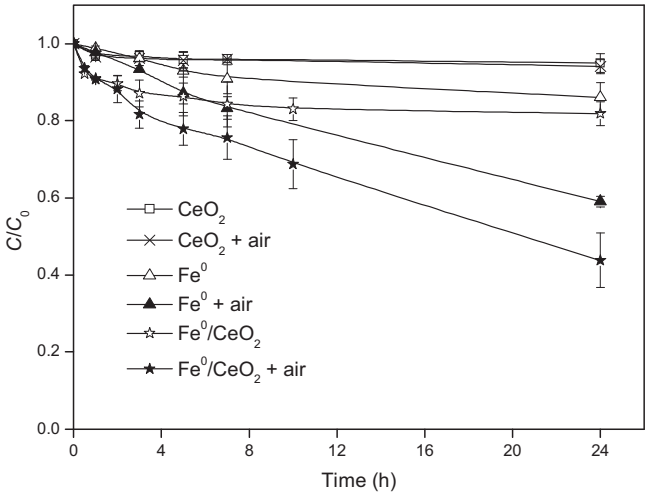

Fig. 7. Removal of 50 mg/L 2,4-DCP with 1.0 g/L CeO_2, Fe^0 or Fe^0/CeO_2 at initial pH 6.2 (not adjusted) and 30 °C under anoxic or oxic conditions.

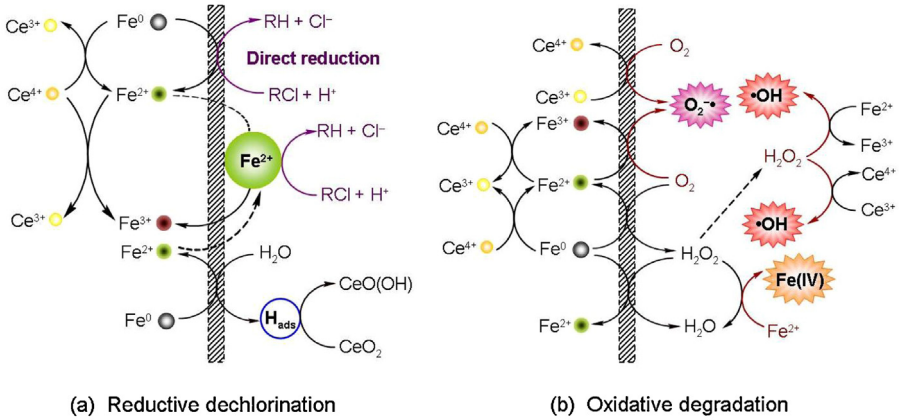

Fig. 8. Reductive and oxidative mechanisms for the removal of chlorophenols with Fe^0/CeO_2 composite under neutral pH conditions.

Eq. (4), cerium oxide easily react with atomic hydrogen, yielding the +4/+3 reduction of Ce with the concurrent oxidation of the H atom and the formation of oxy-hydroxy surface species [56]. The redox couple formed by zero-valent iron Fe^0 and dissolved aqueous Fe^{2+} has a standard reduction potential of −0.44 V, while the standard reduction potential of Ce^{4+}/Ce^{3+} is 1.44 V; thus, the transfer of electrons from Fe^0 to Ce^{4+} represented by Eq. (5) is thermodynamically favorable. It means that the component CeO_2 facilitates the dissolution of Fe^0, producing more dissolved aqueous Fe^{2+}, consistent with our previously reported work [22]. Although Ce^{4+} can also be reduced in a side reaction with Fe^{2+} (Eq. (6)), the facilitation of CeO_2 (Eq. (5)) induces the following indirect dechlorination, finally presenting the slightly enhanced reductive dichlorination of 2,4-DCP (Fig. 7). Hence, a possible reductive mechanism of 2,4-DCP dechlorination by Fe^0/CeO_2 composite is proposed in Fig. 8a.

$$Fe^0 + RCl + H^+ \rightarrow Fe^{2+} + RH + Cl^- \quad (1)$$

$$2Fe^{2+} + RCl + H^+ \rightarrow 2Fe^{3+} + RH + Cl^- \quad (2)$$

$$Fe^0 + 2H_2O \rightarrow Fe^{2+} + 2H_{ads} + 2OH^- \quad (3)$$

$$CeO_2 + H_{ads} \rightarrow CeO(OH) \quad (4)$$

$$Fe^0 + 2Ce^{4+} \leftrightarrow Fe^{2+} + 2Ce^{3+} \quad (5)$$

$$Ce^{4+} + Fe^{2+} \leftrightarrow Ce^{3+} + Fe^{3+} \quad (6)$$

From Fig. 7, in air-equilibrated conditions, the addition of 1.0 g/L Fe^0 and Fe^0/CeO_2 composite removed about 41% and 56% of 2,4-DCP after 24 h. The higher removal efficiency using Fe^0/CeO_2 composite was expected to the enhanced catalytic activity by the introduction of CeO_2. During the removal of 2,4-DCP by Fe^0/CeO_2 composite under oxic condition, 51% of chlorine and 33% of TOC were removed within 24 h. As confirmed by the HPLC and IC analyses, several degradation products, namely phenol, 4-chlorophenol, 2-chlorohydroquinone, hydroxyacetic acid and acetic acid, were detected. Moreover, combined with the XPS and Raman spectra analysis, the adsorption and co-precipitation of dissolved organic compounds and chlorinated organic by-products may also occur on the catalyst surface.

The active species trapping experiments were carried out by adding *n*-butanol (•OH scavenger), *p*-benzoquinone ($O_2^{\bullet-}$ scavenger), and catalase (H_2O_2 scavenger) to the 2,4-DCP degradation solution in the presence of Fe^0/CeO_2 composite (Fig. 9). As it can be seen, the degradation of 2,4-DCP is inhibited by the addition of these three scavengers, indicating the involving of •OH, $O_2^{\bullet-}$ and H_2O_2 species in the 2,4-DCP removal.

On the basis of these results, a possible mechanism during the corrosion of Fe^0/CeO_2 composite in air-saturated water under neutral pH conditions is proposed in Fig. 8b [17,27,28,57]. In the initial step, two electrons transfer from Fe^0 surface to O_2 producing dissolved Fe^{2+} and transient H_2O_2 (Eq. (7)). More Fe^{2+} is formed by another two-electron transfer from Fe^0 to H_2O_2 via the reaction (8). With the introduction of CeO_2, the dissolution of Fe^0 is promoted by the reaction (5), which serves as a source of Fe^{2+} and may be mainly responsible at circumneutral pH. The primary product of Fe^0 corrosion (Eqs. (5), (7) and (8)), Fe^{2+}, reacts with O_2 through a series of one-electron transfer generating $O_2^{\bullet-}$ as well as H_2O_2 (Eqs. (9) and (10)), which occur significantly at neutral pH values [29]. Subsequently, the reaction of Fe^{2+} with H_2O_2 (i.e., Fenton reaction; Eq. (11)) produces highly reactive •OH, whereas the ferryl ion (e.g., FeO^{2+}) is also formed under neutral and basic conditions (Eq. (12)). Furthermore, the chemisorbed oxygen probably trap the electron of Ce^{3+}, and then produces $O_2^{\bullet-}$ by the reaction (13) [48]. Cerium may be capable of redox-cycling with peroxide, and behaves similarly to iron in a Fenton-like reaction, producing •OH through a series of reactions (14)–(16) [22,58], as evidenced by the observation of XPS spectra.

$$Fe^0 + O_2 + 2H^+ \rightarrow Fe^{2+} + H_2O_2 \quad (7)$$

$$Fe^0 + H_2O_2 + 2H^+ \rightarrow Fe^{2+} + 2H_2O \quad (8)$$

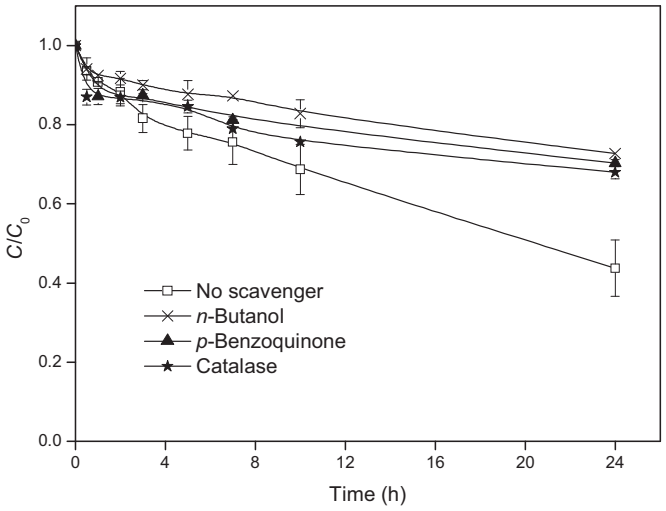

Fig. 9. Removal of 50 mg/L 2,4-DCP with 1.0 g/L Fe^0/CeO_2 composite at initial pH 6.2 and 30 °C in air-saturated water in the presence of *n*-butanol (150 mM), *p*-benzoquinone (1 mM), and catalase (200 U/mL).

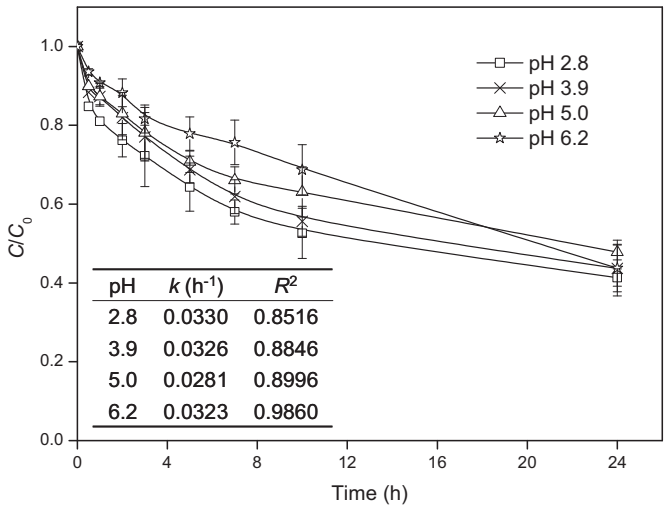

Fig. 10. Effect of initial pH on the removal of 50 mg/L 2,4-DCP with 1.0 g/L Fe^0/CeO_2 composite at 30 °C in air-equilibrated solution, and the table of observed reaction rate constants and corresponding correlation coefficients (inset).

$$Fe^0 + 2Ce^{4+} \leftrightarrow Fe^{2+} + 2Ce^{3+} \quad (5)$$

$$Fe^{2+} + O_2 \rightarrow Fe^{3+} + O_2^{\bullet -} \quad (9)$$

$$Fe^{2+} + O_2^{\bullet -} + 2H^+ \rightarrow Fe^{3+} + H_2O_2 \quad (10)$$

$$Fe^{2+} + H_2O_2 \rightarrow Fe^{3+} + {}^{\bullet}OH + OH^- \quad (11)$$

$$Fe^{2+} + H_2O_2 \rightarrow FeO^{2+} + H_2O \quad (12)$$

$$Ce^{3+} + O_2 \rightarrow Ce^{4+} + O_2^{\bullet -} \quad (13)$$

$$Ce^{3+} + H_2O_2 + H^+ \rightarrow Ce^{4+} + {}^{\bullet}OH + H_2O \quad (14)$$

$${}^{\bullet}OH + H_2O_2 \rightarrow HO_2^- + H_2O \quad (15)$$

$$Ce^{4+} + HO_2^- \rightarrow O_2 + Ce^{3+}H^+ \quad (16)$$

As the solution pH may influence reaction rates directly or indirectly, the removal of 2,4-DCP over a wide range of pH was determined as shown in Fig. 10. The requirement for H^+ participation in a series of reactions (e.g., Eqs. (1), (2), (7) and (8)) implies the possibility that protons may appear in one or more elementary steps that affect the reaction rate directly. Some indirect effects are possible due to increased aqueous corrosion at lower pH values or the precipitation of iron oxides and hydroxides on the composite surface at higher pH values [10,25,28]. The removal of 2,4-DCP at four different pH values of 2.8, 3.9, 5.0 and 6.2, and the observed pseudo-first-order rate constants (k) are shown in Fig. 10. After 24 h of reaction, the finial pH values changed to 5.0, 6.6, 6.9 and 7.1, respectively. Under acidic conditions, increasing H^+ concentration accelerates the corrosion of Fe^0, enhancing the reduction of 2,4-DCP as well as promoting the production of hydroxyl radicals [17,25]. The slightly effect of initial pH value on the degradation of 2,4-DCP was observed over the range of pH 2.8–6.2, possibly due to the dissolution of Fe^0 facilitated by CeO_2 plays a significant role, and the superoxide radicals as well as the ferryl ions are relevant under neutral and basic conditions [17].

3.7. Application of Fe^0/CeO_2 for removal of chlorophenols

The removal of 4-CP, 2,4-DCP, 2,4,6-TCP and PCP were investigated by 1.0 g/L Fe^0/CeO_2 composite at 30 °C in oxic solutions as shown in Fig. 11a. The extent of chlorophenols removal followed the order of PCP > 2,4-DCP > 2,4,6-TCP > 4-CP, which is different from those reported in the removal of various chlorophenols by reductive and oxidative processes. In general, it is observed that the removal rate of chlorophenols decreases with increasing number of chlorine atoms in the aromatic ring [1,2,7,8,59,60]. The dechlorination sequences were 2-CP > 2,4,5-TCP > PCP by magnesium–palladium bimetallic system [8], 4-CP > 2,4-DCP > 2,4,6-TCP by Pd/Fe nanoparticles [2], and monochlorophenols > dichlorophenols > trichlorophenols > pentachlorophenols by Pd/C catalyst [7], respectively. In advanced oxidation processes (AOPs), hydroxyl radicals or other oxidants (e.g., O_3) cause electrophilic reaction attacking aromatic ring, and the degradation sequences were obtained as: 2-CP > 2,4-DCP > 2,4,6-TCP for Fenton's reagent [59], 4-CP > 2-CP > 2,4-DCP > 2,6-DCP > 2,3,5-TCP > 2,4,5-TCP > 2,3,5,6-TeCP > PCP for electro-Fenton process [1], and 4-CP > 2,4-DCP > 2,4,6-TCP > 2,3,4,6-TeCP for both UV radiation and Fenton's reagent [60]. However, some inverse results were observed by many researchers [6,9,60–64]. Ko et al. [9] suggested that the order of reaction rate was 2-CP > 4-CP > 2,4-DCP > 2,4,6-TCP > 2,6-DCP by Ni/Fe bimetallic particles. Patel and Suresh [61] found that dechlorination efficiency and reaction rate constants by magnesium–silver bimetallic system gave the following sequence: PCP > 2,3,4,6-TeCP > 2,4,5-TCP, and Kim and Carraway [6] also reported the same order of pentachlorophenols > tetrachlorophenols > trichlorophenols by zero-valent zinc. Furthermore, the sequences of oxidation rate were 2,3,4,6-TeCP > 2,4,6-TCP > 2,4-DCP > 4-CP for ozonation [60], 2,4-DCP > 2,4,6-TCP > PCP > 4-CP for electro-Fenton method [62], 2,4-DCP > 2-CP > 2,3-DCP > 2,4,6-TCP for photocatalysis [63], and 2-CP > 2,4,6-TCP > 2,4-DCP > PCP for TiO_2/UV [64], respectively.

TOC removal and chloride release during the treatment of chlorophenols by Fe^0/CeO_2 composite were monitored as reported in Fig. 11b and c. In agreement with the changes of chlorophenols concentration found above, the mineralization efficiency (in terms of TOC abatement) and dechlorination rate were observed to decrease in the order of PCP > 2,4-DCP > 2,4,6-TCP > 4-CP. After 24 h of reaction, the mineralization efficiencies were 4%, 33% and 16%, respectively, for 4-CP, 2,4-DCP and 2,4,6-TCP, while the corresponding dechlorination rates were 11%, 51% and 30%. Even when PCP was almost completely removed within 24 h, the mineralization and dechlorination of PCP were 48% and 65%, respectively, indicating that chlorine was not released completely, and chlorinated intermediates were generated in treated solution. Generally, the toxicity of chlorophenols increases with the increasing chlorine substitution [59], so the release of chlorines from the aromatic ring may lower the overall toxicity of chlorophenols. Thus, the treatment with Fe^0/CeO_2 composite in the presence of oxygen could be used as a pretreatment stage to enhance biodegradability and reduce toxicity.

The difference of reactivity sequence obtained from this study might be ascribed to the different types of catalyst and reaction systems (e.g., different electron donor, reaction mechanism). As suggested in the former section, adsorption, co-precipitation, reductive dechlorination, and oxidative degradation of contaminant by Fe^0/CeO_2 composite could occur. The reaction rate of chlorophenols is also largely dependent on both the nature and position of any additional substituent on the ring, which can be described by steric, inductive, and resonance effects [9]. The increasing reactivity of chlorophenols with more atoms of chlorine could be explained by the decreasing C–Cl bond dissociation energy with an increasing number of chlorines [6], and the complex effect of dechlorination, hydroxylation and ring-cleavage functioned in the removal of chlorophenols [60]. However, an exception of 2,4-DCP occurred, that is, 2,4-DCP was removed faster than 2,4,6-TCP. Yuan and Lu [62] gave the interpretation that more steric hindering

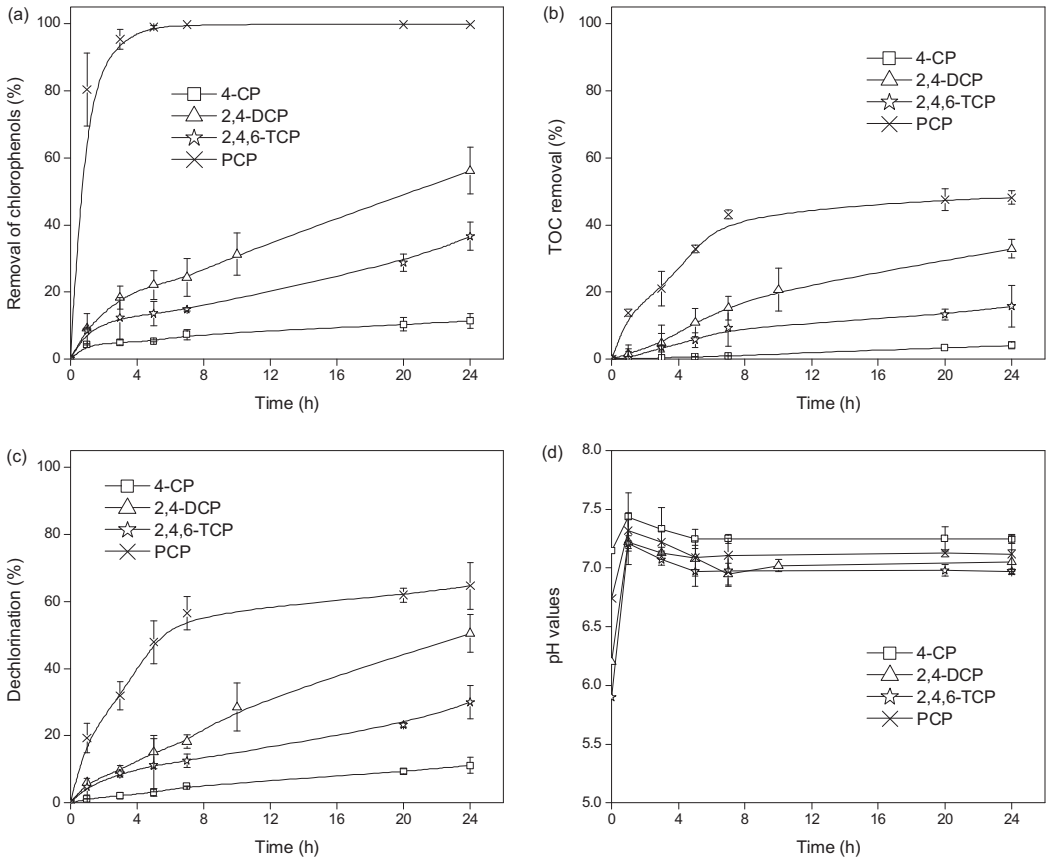

Fig. 11. (a) Removal of 4-CP, 2,4-DCP, 2,4,6-TCP and PCP. (b) Temporal change in TOC removal. (c) Dechlorination of chlorophenols. (d) Evolution of pH values. Reactions were conducted with initial chlorophenols concentration 50 mg/L and Fe^0/CeO_2 composite 1.0 g/L at 30 °C in oxic solutions.

effect was observed on 2,4,6-TCP than 2,4-DCP. More research is required to determine the intermediates for all above chlorophenols and to better understand and verify the complex reaction mechanism.

The removal of chlorophenols were carried out at the original pH of the solutions: 7.1 (4-CP), 6.2 (2,4-DCP), 5.9 (2,4,6-TCP), and 6.7 (PCP). These pH values increased immediately and then stayed at 7.0–7.2 throughout the reaction (Fig. 11d). In the presence of dissolved oxygen, the corrosion of iron and the reduction of water are faster, which increases solution pH according to Eqs. (3) and (17) [65,66]. As a result of iron oxidation, Fe^{2+} formed on the catalyst surface can be further oxidized to Fe^{3+} as described in Eq. (18). Then, Fe^{3+} reacts with H_2O or OH^- yielding oxyhydroxide or hydroxide, and hydroxide can also dehydrate to FeOOH (Eqs. (19) and (20)) [66], which is consistent with the XRD, SEM and Raman results.

$$2Fe^0 + O_2 + 2H_2O \rightarrow 2Fe^{2+} + 4OH^- \quad (17)$$

$$Fe^0 + 2H_2O \rightarrow Fe^{2+} + H_2 + 2OH^- \quad (3)$$

$$4Fe^{2+} + 4H^+ + O_2 \rightarrow 4Fe^{3+} + 2H_2O \quad (18)$$

$$Fe^{3+} + 2H_2O \rightarrow FeOOH + 3H^+ \quad (19)$$

$$Fe^{3+} + 3OH^- \rightarrow Fe(OH)_3 \rightarrow FeOOH + H_2O \quad (20)$$

4. Conclusions

The synthesized Fe^0/CeO_2 composite was composed of spherical Fe^0 particles with grain sizes of 200–400 nm dispersed on cubic fluorite structural CeO_2 matrix. During reaction, the occurrence of Ce^{3+} was observed, and iron was oxidized forming corrosion products possibly associated with lepidocrocite and/or $Fe(OH)_3$. The higher removal efficiency of 2,4-DCP by Fe^0/CeO_2 composite under air-saturated conditions at pH 6.2 resulted from the addition of CeO_2 in the composite that facilitated the dissolution of iron and the generation of comparatively more active surface oxygen species. Reductive dechlorination of 2,4-DCP by Fe^0/CeO_2 composite involved the pathways of direct dechlorination and reduction by Fe^{2+}. The degradation of 2,4-DCP in oxic solutions under neutral conditions was ascribed to the generation of •OH, $O_2^{\bullet -}$, and H_2O_2 species. As for PCP, almost complete removal was observed along with 48% of mineralization and 65% of dechlorination after 24 h of reaction. The removal of chlorophenols followed the order of PCP > 2,4-DCP > 2,4,6-TCP > 4-CP. This Fe^0/CeO_2 composite would be of potential alternative for pretreatment of chlorinated organic contaminants to reduce the effluent toxicity and to enhance biodegradability.

Acknowledgements

The authors are grateful to the precious comments provided by anonymous reviewers.

The authors would also like to acknowledge the financial support provided by the National Natural Science Foundation of China (Grant No. 51078210).

References

[1] N. Oturan, M. Panizza, M.A. Oturan, J. Phys. Chem. A 113 (2009) 10988–10993.
[2] T. Zhou, Y.Z. Li, T.T. Lim, Sep. Purif. Technol. 76 (2010) 206–214.
[3] R. Cheng, J.L. Wang, W.X. Zhang, J. Hazard. Mater. 144 (2007) 334–339.

[4] M.A. Betiha, S.A. Mahmoud, M.F. Menoufy, A.M. Al-Sabagh, Appl. Catal. B: Environ. 107 (2011) 316–326.
[5] L.J. Xu, J.L. Wang, Appl. Catal. B: Environ. 123 (2012) 117–126.
[6] Y.H. Kim, E.R. Carraway, Environ. Technol. 24 (2003) 1455–1463.
[7] C.H. Xia, Y. Liu, S.W. Zhou, C.Y. Yang, S.J. Liu, J. Xu, J.B. Yu, J.P. Chen, X.M. Liang, J. Hazard. Mater. 169 (2009) 1029–1033.
[8] U.D. Patel, S. Suresh, J. Hazard. Mater. 147 (2007) 431–438.
[9] S.O. Ko, D.H. Lee, Y.H. Kim, Environ. Technol. 28 (2007) 583–593.
[10] H. Song, E.R. Carraway, Environ. Sci. Technol. 39 (2005) 6237–6245.
[11] Z.Y. Zhang, M. Lu, Z.Z. Zhang, M. Xiao, M. Zhang, J. Hazard. Mater. 243 (2012) 105–111.
[12] Y. Zhuang, S. Ahn, R.G. Luthy, Environ. Sci. Technol. 44 (2010) 8236–8242.
[13] Y.H. Liou, S.L. Lo, C.J. Lin, W.H. Kuan, S.C. Weng, J. Hazard. Mater. 127 (2005) 102–110.
[14] A.S. Fjordbøge, A. Baun, T. Vastrup, P. Kjeldsen, Chemosphere 90 (2013) 627–633.
[15] S.H. Chang, S.H. Chuang, H.C. Li, H.H. Liang, L.C. Huang, J. Hazard. Mater. 166 (2009) 1279–1288.
[16] Z.Q. Fang, J.H. Chen, X.H. Qiu, X.Q. Qiu, W. Cheng, L.C. Zhu, Desalination 268 (2011) 60–67.
[17] M. Stieber, A. Putschew, M. Jekel, Environ. Sci. Technol. 45 (2011) 4944–4950.
[18] A.S. Reddy, C.Y. Chen, C.C. Chen, S.H. Chien, C.J. Lin, K.H. Lin, C.L. Chen, S.C. Chang, J. Mol. Catal. A: Chem. 318 (2010) 60–67.
[19] A.D. Mayernick, M.J. Janik, J. Phys. Chem. C 112 (2008) 14955–14964.
[20] V.M. Shinde, G. Madras, Appl. Catal. B: Environ. 132–133 (2013) 28–38.
[21] T. Bunluesin, R.J. Gorte, G.W. Graham, Appl. Catal. B: Environ. 15 (1998) 107–114.
[22] L.J. Xu, J.L. Wang, Environ. Sci. Technol. 46 (2012) 10145–10153.
[23] T.S. Zhang, P. Hing, H.T. Huang, J. Kilner, J. Mater. Process. Technol. 113 (2001) 463–468.
[24] T.S. Zhang, J. Ma, L.B. Kong, Z.Q. Zeng, P. Hing, J.A. Kilner, Mater. Sci. Eng., B 103 (2003) 177–183.
[25] L.J. Matheson, P.G. Tratnyek, Environ. Sci. Technol. 28 (1994) 2045–2053.
[26] C. Noubactep, J. Hazard. Mater. 168 (2009) 1626–1631.
[27] C.R. Keenan, D.L. Sedlak, Environ. Sci. Technol. 42 (2008) 6936–6941.
[28] C. Lee, D.L. Sedlak, Environ. Sci. Technol. 42 (2008) 8528–8533.
[29] C.R. Keenan, D.L. Sedlak, Environ. Sci. Technol. 42 (2008) 1262–1267.
[30] L.J. Xu, J.L. Wang, J. Hazard. Mater. 186 (2011) 256–264.
[31] X.Y. Chen, H. Cui, P. Liu, G.W. Yang, Chem. Mater. 20 (2008) 2035–2038.
[32] X.F. Tang, Y.G. Li, X.M. Huang, Y.D. Xu, H.Q. Zhu, J.G. Wang, W.J. Shen, Appl. Catal. B: Environ. 62 (2006) 265–273.
[33] K. Gupta, S. Bhattacharya, D. Chattopadhyay, A. Mukhopadhyay, H. Biswas, J. Dutta, N.R. Ray, U.C. Ghosh, Chem. Eng. J. 172 (2011) 219–229.
[34] J.W. Gaffney, K.N. White, S. Boult, Environ. Sci. Technol. 42 (2008) 3575–3581.
[35] Y.H. Huang, T.C. Zhang, Water Res. 40 (2006) 3075–3082.
[36] L.F. Greenlee, J.D. Torrey, R.L. Amaro, J.M. Shaw, Environ. Sci. Technol. 46 (2012) 12913–12920.
[37] M. Kruk, M. Jaroniec, Chem. Mater. 13 (2001) 3169–3183.
[38] S.K. Meher, G.R. Rao, J. Colloid Interface Sci. 373 (2012) 46–56.
[39] F. Duarte, F.J. Maldonado-Hódar, A.F. Pérez-Cadenas, L.M. Madeira, Appl. Catal. B: Environ. 85 (2009) 139–147.
[40] A.N. Mansour, C.A. Melendres, J. Electrochem. Soc. 142 (1995) 1961–1968.
[41] W.L. Yan, A.A. Herzing, X.Q. Li, C.J. Kiely, W.X. Zhang, Environ. Sci. Technol. 44 (2010) 4288–4294.
[42] M. Dickinson, T.B. Scott, J. Hazard. Mater. 178 (2010) 171–179.
[43] J.S. Cao, X.Q. Li, J. Tavakoli, W.X. Zhang, Environ. Sci. Technol. 42 (2008) 3780–3785.
[44] X.Q. Li, W.X. Zhang, J. Phys. Chem. C 111 (2007) 6939–6946.
[45] P. Burroughs, A. Hamnett, A.F. Orchard, G. Thornton, J. Chem. Soc. Dalton (1976) 1686–1698.
[46] B.M. Reddy, A. Khan, Y. Yamada, T. Kobayashi, S. Loridant, J.C. Volta, J. Phys. Chem. B 107 (2003) 5162–5167.
[47] H.L. Li, C.Y. Wu, Y. Li, J.Y. Zhang, Environ. Sci. Technol. 45 (2011) 7394–7400.
[48] S.X. Yang, W.P. Zhu, Z.P. Jiang, Z.X. Chen, J.B. Wang, Appl. Surf. Sci. 252 (2006) 8499–8505.
[49] Y. Zhang, M. Yang, X.M. Dou, H. He, D.S. Wang, Environ. Sci. Technol. 39 (2005) 7246–7253.
[50] Z.J. Li, S.B. Deng, G. Yu, J. Huang, V.C. Lim, Chem. Eng. J. 161 (2010) 106–113.
[51] X.B. Hu, B.Z. Liu, Y.H. Deng, H.Z. Chen, S. Luo, C. Sun, P. Yang, S.G. Yang, Appl. Catal. B: Environ. 107 (2011) 274–283.
[52] S. Kushwaha, B. Sreedhar, P. Padmaja, Langmuir 28 (2012) 16038–16048.
[53] L.J. Oblonsky, T.M. Devine, Corros. Sci. 37 (1995) 17–41.
[54] K.C.K. Lai, I.M.C. Lo, Environ. Sci. Technol. 42 (2008) 1238–1244.
[55] W. Song, X.H. Shang, Y. Lu, B.B. Liu, X. Wang, Chem. Res. Chin. Univ. 27 (2011) 854–856.
[56] G. Vicario, G. Balducci, S. Fabris, S. de Gironcoli, S. Baroni, J. Phys. Chem. B 110 (2006) 19380–19385.
[57] S.Y. Pang, J. Jiang, J. Ma, Environ. Sci. Technol. 45 (2011) 307–312.
[58] E.G. Heckert, S. Seal, W.T. Self, Environ. Sci. Technol. 42 (2008) 5014–5019.
[59] W.Z. Tang, C.P. Huang, Chemosphere 33 (1996) 1621–1635.
[60] F.J. Benitez, J. Beltran-Heredia, J.L. Acero, F.J. Rubio, Chemosphere 41 (2000) 1271–1277.
[61] U. Patel, S. Suresh, J. Colloid Interface Sci. 299 (2006) 249–259.
[62] S.H. Yuan, X.H. Lu, J. Hazard. Mater. 118 (2005) 85–92.
[63] J. Bandara, J.A. Mielczarski, A. Lopez, J. Kiwi, Appl. Catal. B: Environ. 34 (2001) 321–333.
[64] L.F. González, V. Sarria, O.F. Sánchez, Bioresour. Technol. 101 (2010) 3493–3499.
[65] H. Choi, S.R. Al-Abed, S. Agarwal, Environ. Sci. Technol. 43 (2009) 4137–4142.
[66] X.Q. Li, D.W. Elliott, W.X. Zhang, Crit. Rev. Solid State Mater. Sci. 31 (2006) 111–122.